# Bridging the Gap between Small Clusters and Nanodroplets: Spectroscopic Study and Computer Simulation of Carbon Dioxide Solvated with Helium Atoms

J. Tang,[1] A. R.W. McKellar,[1] F. Mezzacapo,[2] and S. Moroni[2]

[1]*Steacie Institute for Molecular Sciences, National Research Council of Canada, Ottawa, Ontario, Canada K1A 0R6*
[2]*SMC INFM, Dipartimento di Fisica, Università di Roma La Sapienza, Piazzale Aldo Moro 2, I-00185 Rome, Italy*
(Received 27 November 2003; published 8 April 2004)

High resolution infrared spectra of $He_N$-$CO_2$ clusters with $N$ up to 17 have been studied in the region of the $CO_2$ $\nu_3$ fundamental band. The $B$ rotational constant initially drops as expected for a normal molecule, reaching a minimum for $N = 5$. Its subsequent rise for $N = 6$ to 11 can be interpreted as the transition from a normal (though floppy) molecule to a quantum solvation regime. For $N > 13$, the $B$ value becomes approximately constant with a value about 17% larger than that measured in much larger helium nanodroplets. Quantum Monte Carlo calculations of pure rotational spectra are in excellent agreement with the measured $B$ in this size range and complement the experimental study with detailed structural information. For a larger cluster size ($N = 30$–50) the simulations show a clear sign of convergence towards the nanodroplet $B$ value.

DOI: 10.1103/PhysRevLett.92.145503 PACS numbers: 61.46.+w, 02.70.Ss, 36.40.Mr

Helium clusters offer the possibility of studying manifestations of superfluidity at a microscopic scale and, more generally, effects of confinement in quantum fluids [1]. Superfluidity can be defined and measured in terms of the response to an external perturbation [2,3]. While path integral Monte Carlo calculations found superfluidity behavior in $^4$He droplets with as few as 64 atoms [4], direct experimental evidence of superfluidity in pure He clusters has remained elusive. In recent years He nanodroplet isolation (HENDI) spectroscopy [5] has made a probe to rotational motion in He droplets available. Spectroscopic interrogation of molecules solvated in $^4$He droplets reveals free-rotor-like spectra [6], although with an increased moment of inertia. Theoretical descriptions, based on demotion of superfluidity in the first solvation shell induced by the anisotropy and strength of the molecule-He potential [7,8] and on hydrodynamic response of the modulated superfluid density around the molecule [9], give a fairly good account for the increased moment of inertia observed in large droplets (from a few hundred to the order of ten thousands of He atoms), especially for relatively heavy and slow rotors such as $SF_6$ and carbonyl sulfide (OCS). However, the relative importance of different effects is still under debate.

Recently, measurements of the evolution of rotational constants with the size of the cluster have been reported [10,11]. For $^4He_N$-OCS, $B$ decreases in the range $N < 8$, undershooting its nanodroplet value, which implies a subsequent turnaround at larger cluster sizes [10]. Quantum Monte Carlo (QMC) calculations of rotational excitations of the cluster confirm the observed undershoot, locating the minimum of $B$ at $N = 6$ [12] or 8–9 [13]. Experimentally, such a turnaround has been observed in $^4He_N$-$N_2O$, with a first minimum of $B$ at $N = 6$, followed by an oscillatory behavior [11]. For $N_2O$, however, the value of $B$ obtained for all clusters for $N$ up to 12 is significantly above its nanodroplet limit [14]. Slow convergence of $B$ has been predicted for light rotors such as HCN [15], but it is somewhat unexpected for $N_2O$, which is in several respects similar to OCS. Whether this is related to the anomalously low value of $B$ of the $N_2O$ molecule measured in large droplets [14] is presently not understood.

In the present Letter, we use $CO_2$ as the probe molecule and further extend the study of small helium clusters (i) by recording infrared spectra in the region of the $CO_2$ $\nu_3$ fundamental band (2350 cm$^{-1}$) and (ii) by calculating the rotational spectrum in the vibrational ground state by means of QMC simulations.

In many respects, $CO_2$ is similar to $N_2O$ and OCS. But, of course, there is also a significant difference: $CO_2$ is symmetric and nonpolar. Because of symmetry, only half of the normal rotational levels of ground-state $^{12}C^{16}O_2$ molecules are occupied (odd $J$ values are forbidden), with the result that $He_N$-$CO_2$ cluster spectra are simpler and less congested than those of $He_N$-$N_2O$ and $He_N$-OCS. But these missing rotational transitions also mean that the spectra contain less information. The net effect is that we can more easily follow the pattern of $He_N$-$CO_2$ transitions to high $N$ values ($N = 17$, which is considerably higher than for $He_N$-$N_2O$ and $He_N$-OSC), but the resulting rotational assignment and analysis is less secure and precise. While confirmation of infrared assignments from observations of analogous pure rotational microwave transitions is not possible for $CO_2$ as it was for $N_2O$ and OCS, the agreement with the theoretical simulations reported here strongly support the experimental analysis.

The apparatus was similar to that used previously in our work on He clusters [10,16]. A tunable infrared diode laser is used to probe a pulsed supersonic jet expansion. The gas mixtures consist of very small concentrations (0.1% to 0.002%) of $CO_2$ in ultrahigh purity helium. We use both pinhole- and slit-shaped jet nozzles, with temperatures varied from $-20$ to $-160\,^\circ$C, and rather high

 © 2004 The American Physical Society 

backing pressures up to about 45 atm. The $N$-value assignments were primarily based on the order in which the lines appear as clustering is increased in the supersonic expansion by raising backing pressure and lowering jet temperature. The assignments were also supported by the rotational analyses, as described below. Finally, they were partly based on achieving a smooth behavior of line position as a function of $N$.

Details of the assignments will be reported elsewhere [17]. We discuss here the rotational analysis. Three transitions, $R(0)$, $P(2)$, and $R(2)$, were assigned for each cluster with $N$ between 3 and 17 [18]. These limited data can be fitted in terms of at most three parameters. The only practical approach is to use the simple linear molecule energy expression, $E = \nu_0 + BJ(J+1) - D[J(J+1)]^2$, to determine the band origin, $\nu_0$, rotational constant, $B$, and centrifugal distortion constant, $D$, assuming that $B$ and $D$ are the same in the ground and excited vibrational states, $\nu_3(CO_2) = 0$ and 1.

The variation of the vibrational band origin, $\nu_0$, with cluster size is shown in Fig. 1(a), which includes a comparison with $He_N$-OCS and $He_N$-$N_2O$. All three cluster systems show the same turnaround in vibrational shift at $N = 5$, which can be explained by the donut model in which the first five He atoms occupy equivalent positions around the equator of the $CO_2$, OCS, or $N_2O$, where each exerts a similar blueshifting effect. Subsequent He atoms occupy positions closer to the ends of the molecule, where they exert a redshifting effect on the vibration. The very close match between the $CO_2$ and OCS shifts for $N = 1$ to 8 in Fig. 1(a) is quite remarkable, and this helps to support the present analysis for $N = 3$ to 8. Unfortunately, we cannot compare the present vibrational shifts with that of $CO_2$ in helium nanodroplets since our observations were in the $\nu_3$ fundamental band region, while the only available nanodroplet observations apply to the $\nu_1 + \nu_3$ and $2\nu_2 + \nu_3$ bands [14].

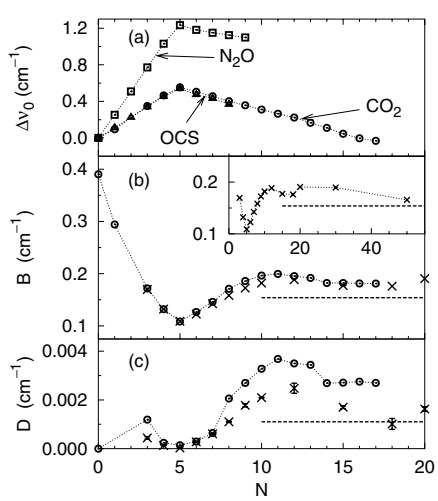


FIG. 1. Variation with the cluster size of (a) the vibrational band origin, $\Delta\nu_0$, (b) the rotational constant, $B$, and (c) the centrifugal distortion constant, $D$. Circles and crosses indicate, respectively, the present experimental and theoretical results for $He_N$-$CO_2$. Panel (a) includes for comparison the value of $\Delta\nu_0$ for $He_N$-OCS [10] and $He_N$-$N_2O$ [11]. The inset of panel (b) shows the calculated $B$ values in an extended range. The dashed lines indicate the nanodroplet results [14].

The variation of $B$ rotational constant with $N$ is shown in Fig. 1(b). Starting at the value for the isolated $CO_2$ molecule, 0.39 cm$^{-1}$, $B$ drops to a minimum of 0.11 cm$^{-1}$ at $N = 5$ and then rises through a broad local maximum of 0.20 cm$^{-1}$ around $N = 11$, signaling a transition to a regime where a fraction of the helium density is decoupled from the rotation of the molecule [11–13]. For $N = 14$ to 17, $B$ decreases slightly to an almost constant value of 0.18 cm$^{-1}$. The limiting large-$N$ value for helium nanodroplets [14], $B = 0.154$ cm$^{-1}$, is indicated by a dashed line in Fig. 1(b), and it appears that the leveling of the $B$ value between $N = 14$ and 17 is not an indication of saturation; indeed further structure is revealed by the theoretical results for larger clusters (see below). For $He_N$-OCS, $B$ decreases steadily from $N = 0$ to 8, passing through the nanodroplet value at about $N = 5$, and its eventual turnaround has not yet been observed experimentally [10]. For $He_N$-$N_2O$, the variation of $B$ is rather similar to that of $He_N$-$CO_2$, but with the significant difference that $B$ always remains above its nanodroplet value for $He_N$-$N_2O$ [11]. The $He_N$-$CO_2$ and $He_N$-$N_2O$ rotational parameters are almost identical for $N = 1$, 3, 4, and 5. A significant deviation starts for $N = 6$, where the $B$ value of $He_N$-$CO_2$ rises while that of $He_N$-$N_2O$ continues to fall [11]. It is tempting to relate this difference to symmetry: the donut ring having been filled with five He atoms, the sixth atom can go to the preferred end of $N_2O$. But it has no such easy choice with $CO_2$, where it must divide itself between the two ends. This has the effect of destabilizing the ring. Evidently, the OCS, $N_2O$, and $CO_2$ molecules behave rather differently in small helium clusters in spite of their close family ties, as already known for larger clusters from HENDI spectroscopy [14]. In general terms, the fact that $He_N$-$CO_2$ shows the earliest and most pronounced $B$ value turnaround, compared to the other family members, is not surprising in view of its higher symmetry and the weaker anisotropy of its interaction with helium [19–21].

Figure 1(c) shows the variation with $N$ of the centrifugal distortion parameters, $D$. We can compare these values with those determined previously for $He_N$-OCS and $He_N$-$N_2O$ clusters [10,11]. For $N = 3$ to 7, the $He_N$-OCS distortion parameters are considerably smaller, while those of $He_N$-$N_2O$ are similar to those of $He_N$-$CO_2$. This similarity tends to support the present analysis; other possible assignments gave less reasonable $D$ values. For $N = 8$ and larger, the present experimental $D$ values jump into the range 0.0020–0.0035 cm$^{-1}$, which is quite large compared to $He_N$-$N_2O$ [11], or to $CO_2$ in nanodroplets [14], both of which have $D \approx 0.001$ cm$^{-1}$. But the agreement between experiment and theory is still satisfactory, particularly in view of experimental uncertainties arising

from the sparse nature of the data and the simple three parameter fits.

We turn now to the presentation of the QMC calculation. The simulations are performed with the reptation QMC algorithm [22], using recent *ab initio* results for both the He-He interaction [23] and the He-$CO_2$ potential energy surface (PES) in the vibrational ground state of the molecule [19]. Details of the simulations are similar to those of Ref. [13] and need not be repeated here. The estimates of the ground-state energy of the clusters and the He density profiles $\rho(\mathbf{r})$ are exact, for given interparticle interactions, within known statistical errors. The calculation of the rotational spectrum is less straightforward. For a cluster with a given $N$, the simulation gives unbiased estimates for the imaginary-time correlation functions $c_J(\tau) = \langle P_J[\mathbf{n}(\tau) \cdot \mathbf{n}(0)]\rangle$, where $P_J[\cos(\theta)]$ are Legendre polynomials, $\mathbf{n}(\tau)$ is the versor of the molecular axis at imaginary time $\tau$, and $\langle\,\rangle$ denotes a ground-state average. The energies of the eigenstates of the cluster with total angular momentum $J$, involving molecular rotation, are then obtained from a fit to $c_J(\tau)$ [13]. Finally, excitation energies at different values of $J$ are analyzed in terms of a linear rotor model, yielding the rotational constant $B$ and the distortion parameter $D$. The analytic continuation of imaginary-time correlation functions is in general an ill-conditioned problem [24]. However, the experimental observation that the rotational spectrum of the cluster is well represented by a free linear rotor implies that for given $J$ there is a strong peak well separated in energy from other spectral features. In these conditions, the position of the peak inferred from imaginary-time correlations is fairly robust against details of the fitting procedure. Success of a similar analysis for $He_N$-OCS and $He_N$-$N_2O$ clusters [13,25] further supports the reliability of the procedure.

The He density profiles for $He_N$-$CO_2$ clusters with $N = 5$ and 6 are compared in Fig. 2 with those of $He_N$-OCS [26] and $He_N$-$N_2O$ [25]. The structural information (donut model) contained in the turnaround of the measured vibrational shift at $N = 5$ for all these clusters is clearly demonstrated: the first five atoms fill an equatorial ring around the molecule, and the sixth spills out towards the poles of the molecule, leaving the density in the ring essentially unchanged. For $He_6$-$CO_2$ the density outside the donut is evenly distributed, owing to both the symmetry and the shape of the PES (for $CO_2$, secondary minima of the potential at the molecular poles are shallower than for OCS [20] or $N_2O$ [21] on the oxygen side). The effect of the sixth atom in destabilizing the ring, experimentally observed as a reduction of the moment of inertia, can be characterized in terms of the molecule-atom angular motion correlation $\phi(\mathbf{r}) = -\langle \mathbf{L} \cdot \mathbf{l}(\mathbf{r})\rangle$, where $\mathbf{L}$ indicates the angular momentum of the $CO_2$ molecule, and $\mathbf{l}(\mathbf{r})$ is the angular current operator of He atoms at point $\mathbf{r}$ [13]. A large value of $\phi(\mathbf{r})$ means that the local He density tends to follow the molecular rotation. We find that for the $He_6$-$CO_2$ cluster $\phi(\mathbf{r})$ is zero, within statistical noise, outside the ring, and significantly lower than for $N = 5$ in the donut region. Therefore the "wings" of density which appear for $N = 6$ do not give any local contribution to the moment of inertia; furthermore, their presence has the effect of decoupling from molecular rotation some of the density present in the donut region (making permutation cycles with a large projected area more likely [8]). For $He_6$-OCS and $He_6$-$N_2O$, on the other hand, localization of the density in the polar angular coordinate accounts for the observed increase of the moment of inertia from $N = 5$ to 6 [10,11].

Further structural information is obtained from the ground-state energy of the clusters, $E(N)$. Figure 3 shows the incremental binding energy per added He atom, $E(N) - E(N-1)$ {approximated as $[E(N_i) - E(N_j)]/(N_i - N_j)$ when simulations for consecutive values of $N$ have not been done}. Once again, the fact that the first five He atoms occupy equivalent positions is manifest. Also clear, both in the incremental binding energy and in the

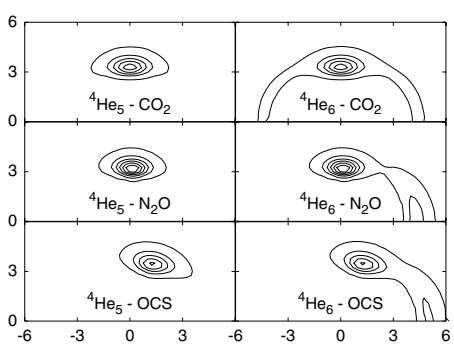


FIG. 2. Contour plot of the helium density profile in a plane containing the molecular axis, for clusters of 5 and 6 helium atoms. The molecule (either $CO_2$, $N_2O$ [25], or OCS [26]) has its center of mass at the origin and an oxygen atom on the positive $x$ directon. Distances are in angstroms, and contour levels start at 0.002 with increments of 0.010, in units of inverse cubic angstroms.

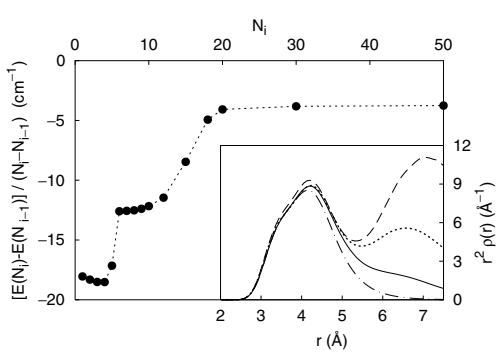


FIG. 3. Incremental binding energy per added helium atom for $He_N$-$CO_2$ clusters (top and left scales). Statistical errors are smaller than the symbol size. The inset shows the radial distribution of the He density (bottom and right scales) for $N = 15$ (dash-dotted line), 20 (solid line), 30 (dotted line), and 50 (dashed line).

radial distribution $r^2\rho(r)$ of the He density, shown in the inset of Fig. 3, is the signature of the first solvation shell completion before $N = 20$.

Finally we compare in Figs. 1(b) and 1(c) the measured and calculated values of the rotational constant $B$ and centrifugal distortion $D$. For all the cluster sizes where both experimental and theoretical values have been determined, the agreement for $B$ is almost perfect — the main difference being a small theoretical underestimate of the broad maximum around $N = 11$. Note that the simulations for $N$ up to 15 were performed without prior knowledge of the experimental results. The calculated centrifugal distortions are generally smaller than those obtained from the rotational analysis of the measured spectra. However, both the general trend of the dependence on the cluster size and the very large value of $D$ compared to the OCS- and $N_2O$-doped cluster are well reproduced. In view of the uncertainties inherent in a rotational analysis with rather sparse data, we consider the overall agreement quite gratifying. For larger cluster sizes, the theoretical value of the rotational constant rises again at $N = 20$, corresponding to completion of the first solvation shell, and (assuming one can interpolate smoothly between rather distant values of $N$) begins to approach the nanodroplet limit by $N = 50$.

In summary we have determined the effective rotational constant $B$ of $He_N$-$CO_2$ clusters using both high resolution infrared spectroscopy and computer simulation. We stress the impressive agreement obtained with completely independent experimental and theoretical methods. The main feature to emerge is the $B$-value turnaround at $N = 5$, earlier (lower $N$), sharper, and more dramatic than in He-$N_2O$ and $He_N$-OCS. We conclude with a few comments on the results reported. First, the quality of the He-$CO_2$ PES [19] employed here is quite remarkable. This suggests that measurements and simulations of medium-large size clusters can be useful in general to gauge the accuracy of PES and should motivate accurate calculations of helium-molecule interactions in vibrationally excited states for reliable theoretical studies of vibrational shifts. Second, lacking confirmation from pure rotational microwave transitions for $CO_2$, the present infrared line assignments were partly based on assumptions such as the smooth behavior as a function of $N$ and the independence of the rotational constants on the vibrational state of the molecule. The excellent agreement with the completely independent simulation results supports these assumptions and gives confidence in the assignments. Third, the experimental determination of the rotational constant, up to a number of helium atoms close to completion of the first solvation shell, gives a value still significantly higher than its nanodroplet limit. This extends to larger cluster sizes (and QMC simulations push even further) a similar result previously observed in $He_N$-$N_2O$ [11], suggesting that a nontrivial evolution of the $B$ value beyond the first solvation shell might be a rather common property.

We thank G. Scoles and S. Baroni for stimulating discussions. We acknowledge the allocation of computer resources from INFM Iniziativa Calcolo Parallelo.

[1] S. A. Chin and E. Krotscheck, Phys. Rev. B **52**, 10 405 (1995).
[2] G. Baym, in *Mathematical Methods in Solid State and Superfluid Theory*, edited by R. C. Clark and E. H. Derrick (Oliver and Boyd, Edinburgh, 1969), p. 121.
[3] E. L. Andronikashvili, J. Phys. (Moscow) **10**, 201 (1946).
[4] P. Sindzingre, M. L. Klein, and D. M. Ceperley, Phys. Rev. Lett. **63**, 1601 (1989).
[5] C. Callegari, K. K. Lehmann, R. Schmied, and G. Scoles, J. Chem. Phys. **115**, 10 090 (2001).
[6] S. Grebenev, J. P. Toennies, and A. F. Vilesov, Science **279**, 2083 (1998).
[7] Y. Kwon, P. Huang, M.V. Patel, D. Blume, and K. B. Whaley, J. Chem. Phys. **113**, 6469 (2000).
[8] E.W. Draeger and D. M. Ceperley, Phys. Rev. Lett. **90**, 065301 (2003).
[9] C. Callegari *et al.*, Phys. Rev. Lett. **83**, 5058 (1999).
[10] J. Tang, Y. Xu, A. R.W. McKellar, and W. Jäger, Science **297**, 2030 (2002); Y. Xu and W. Jäger, J. Chem. Phys. **119**, 5457 (2003); J. Tang and A. R.W. McKellar, *ibid.* **119**, 5467 (2003).
[11] Y. Xu, W. Jäger, J. Tang, and A. R.W. McKellar, Phys. Rev. Lett. **91**, 163401 (2003).
[12] F. Paesani *et al.*, Phys. Rev. Lett. **90**, 073401 (2003).
[13] S. Moroni *et al.*, Phys. Rev. Lett. **90**, 143401 (2003).
[14] K. Nauta and R. E. Miller, J. Chem. Phys. **115**, 10 254 (2001).
[15] A. Viel and K. B. Whaley, J. Chem. Phys. **115**, 10 186 (2001).
[16] J. Tang and A. R.W. McKellar, J. Chem. Phys. **119**, 754 (2003).
[17] J. Tang and A. R.W. McKellar (to be published).
[18] The binary complex, He-$CO_2$, was studied previously: M. J. Weida *et al.*, J. Chem. Phys. **101**, 8351 (1994).
[19] T. Korona, R. Moszynski, F. Thibault, J.-M. Launay, B. Bussery-Honvault, J. Boissoles, and P. E. Wormer, J. Chem. Phys. **115**, 3074 (2001).
[20] J. M. M. Howson and J. M. Hutson, J. Chem. Phys. **115**, 5059 (2001).
[21] (a) B. T. Chang, O. Akin-Ojo, R. Bukowski, and K. Szalewicz, J. Chem. Phys. **119**, 11 654 (2003); (b) X. Song, Y. Xu, P. N. Roy, and W. Jäger (to be published).
[22] S. Baroni and S. Moroni, Phys. Rev. Lett. **82**, 4745 (1999).
[23] T. Korona *et al.*, J. Chem. Phys. **106**, 5109 (1997).
[24] J. E. Gubernatis and M. Jarrell, Phys. Rep. **269**, 135 (1996).
[25] S. Moroni, N. Blinov, and P. N. Roy (to be published).
[26] For the OCS dopant, $\rho(r)$ is calculated with the *unmorphed* version of the PES of Ref. [20]. Morphing the potential causes some of the He density to leak on the sulfur side [13] for $N = 6$. Using the unmorphed PES we find significantly better agreement with the experimental value [10] of $B$ for $N > 5$.